NANO LETTERS

Letter

pubs.acs.org/NanoLett

Ultraviolet Nanoplasmonics: A Demonstration of Surface-Enhanced Raman Spectroscopy, Fluorescence, and Photodegradation Using Gallium Nanoparticles

Yang Yang,[†] John M. Callahan,[‡] Tong-Ho Kim,[§] April S. Brown,[§] and Henry O. Everitt*[,†,§,∥]

[†]Department of Physics, Duke University, Durham, North Carolina 27708, United States

[‡]AEgis Technologies Group, Inc., 410 Jan Davis Drive, Huntsville, Alabama 35806, United States

[§]Department of Electrical and Computer Engineering, Duke University, Durham, North Carolina 27708, United States

[∥]Army Aviation and Missile RD&E Center, Redstone Arsenal, Alabama 35898, United States

ABSTRACT: Self-assembled arrays of hemispherical gallium nanoparticles deposited by molecular beam epitaxy on a sapphire support are explored as a new type of substrate for ultraviolet plasmonics. Spin-casting a 5 nm film of crystal violet upon these nanoparticles permitted the demonstration of surface-enhanced Raman spectra, fluorescence, and degradation following excitation by a HeCd laser operating at 325 nm. Measured local Raman enhancement factors exceeding 10^7 demonstrate the potential of gallium nanoparticle arrays for plasmonically enhanced ultraviolet detection and remediation.

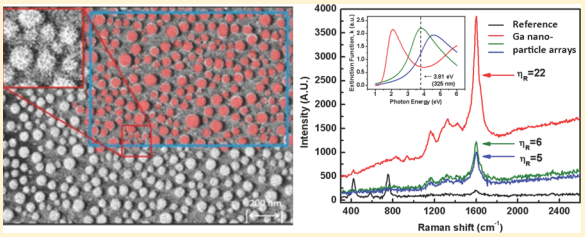

KEYWORDS: *Ultraviolet, plasmonics, gallium, nanoparticles, surface-enhanced Raman, surface-enhanced fluorescence*

Most current research in plasmonics employs gold or silver nanostructures whose localized surface plasmon resonances (LSPRs) constrain their use to the infrared or visible spectral regions.[1−4] Surface-enhanced Raman spectroscopy (SERS), fluorescence (SEF), and photodegradation (SEPD) use LSPRs to enhance scattering and absorption cross sections by many orders of magnitude, providing sensitive detection and efficient remediation of analytes.[5−9] Applications such as these would benefit from LSPRs in the ultraviolet (UV) spectral region;[10−15] for example, Raman scattering cross sections increase as the fourth power of laser frequency.[16,17] Among metals with UV LSPRs,[10,12,18] nanoparticles (NPs) of gallium are of particular interest because of their facile synthesis, widely tunable UV LSPR, and minimal oxidation.[19−22] Here we demonstrate UV SERS, SEF, and SEPD of a prototypical analyte (crystal violet) deposited on Ga NPs and report the first UV local enhancement factors comparable to those routinely achieved with gold or silver NPs (>10^7).[18,23,24]

Controlled synthesis of Ga NPs on sapphire substrates using molecular beam epitaxy (MBE) deposition has been recently reported.[20,25] Because the Ga NPs form as liquid droplets under this growth condition, they tend to form close-packed self-similar truncated hemispheroids. The NP ensemble is characterized by a unimodal or a bimodal size distribution whose mean diameter(s) increase(s) with increasing deposition time.[20] A set of three such samples, consisting of sapphire-deposited Ga ensembles of increasing mean NP diameter, was fabricated as UV nanoplasmonic substrates for this demonstration. The scanning electron microscope (SEM) imagery in Figure 1a,b,c indicates that the bimodal size distribution emerges as larger NPs grow through coalescence, leaving behind a halo of smaller NPs in the interstitial spaces.

In these studies, we used spectroscopic ellipsometry (SE) to monitor the LSPR spectra during NP deposition, observing the extinction peak associated with the LSPR absorption to redshift with increasing deposition time as the Ga NPs grow larger in size.[20,21,25] The smaller NPs do not contribute significantly to the LSPR measured by grazing incidence spectroscopic ellipsometry (SE) because of their inefficient absorption and shadowing by the larger NPs. Deposition can be halted when the LSPR peak reaches the desired frequency, which for SERS, SEF, and SEPD is expected to be near the frequency of the laser.[26] The measured LSPR peak represents the collective LSPR absorption profiles of the constituent interacting Ga NPs, and the inhomogeneous distribution of NP sizes can broaden and frequency-shift the LSPR resonance accordingly.

Grazing incidence SE of Ga NPs reveals two LSPR modes that redshift with increasing NP size. Recent theoretical analysis of hemispherical Ga NPs on sapphire using a discrete dipole approximation (DDA) confirms experimental evidence that coupling of the s-polarized component to the transverse dimension of the NP produces the lower frequency LSPR mode, while the p-polarized component couples mostly to the shorter vertical dimension of the NP and produces the higher frequency LSPR mode.[20,27] By contrast, for near-normal incidence typical of spectroscopic measurements the degener-

Received: March 30, 2013
Revised: May 6, 2013
Published: May 9, 2013

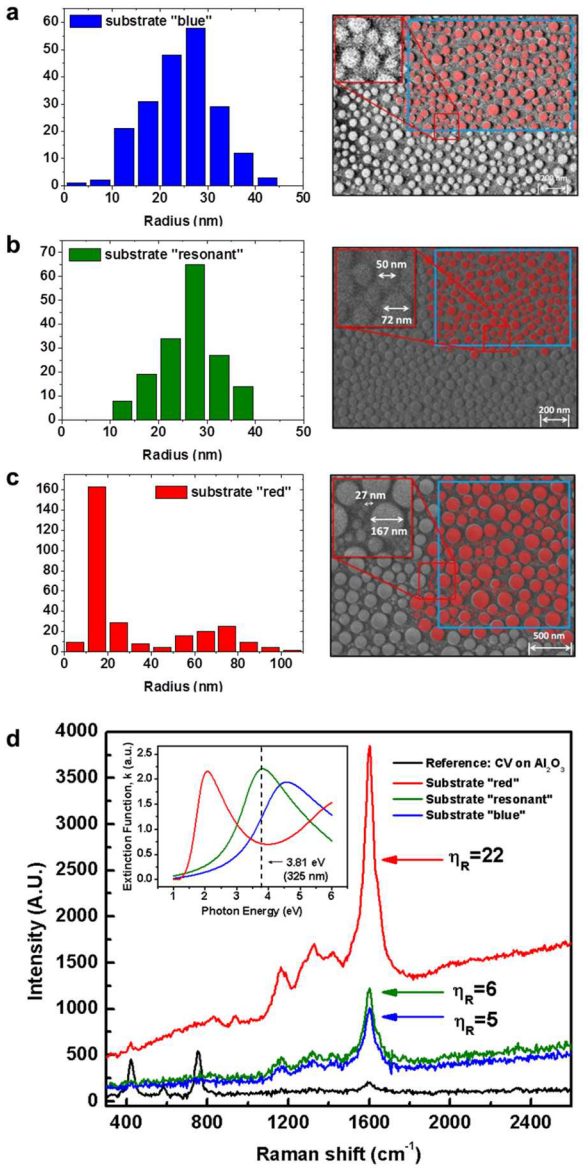

Figure 1. Size distribution and SEM imagery of the "blue" (a), "resonant" (b), and "red" (c) SERS substrates. Measured CV SERS (d) from the three substrates compared to the Raman signal from CV on bare sapphire. The inset shows the LSPR of the three substrates and the 3.81 eV laser energy.

ate s- and p-polarized (lower frequency) modes couple only to the transverse dimension of the NPs, while the higher frequency mode disappears.

The measured SE spectra of the three substrates (Figure 1d inset) indicate that the "lower frequency" LSPR peaks were chosen to be on the blue side of (4.5 eV), nearly coincident with (3.80 eV), or on the red side of (1.95 eV) the 5 mW continuous wave HeCd UV laser wavelength of 325 nm (3.81 eV). The mean NP radius (23 nm, 26 nm, and 70 nm, respectively) increased with decreasing LSPR frequency. The hemispherical Ga NPs, whose varying widths and corresponding heights constituted the surface-supported ensemble, covered about half the sapphire surface. The "blue" and "resonant" substrates exhibited unimodal size distributions, but the "red" substrate exhibited a bimodal size distribution, 70% of whose smaller NPs (16 nm mean radius) were within 12 nm of a large NP. For reference during spectroscopic measurements, a portion of each substrate was covered during deposition to expose bare sapphire ex situ. Spectroscopic measurements were performed on both covered and bare portions in order to compare the relative Raman and fluorescence strengths.

Crystal violet (CV) was chosen as the Raman-active analyte, a dye susceptible to damage by UV illumination that exhibits peak fluorescence near 590 nm and only weak fluorescence near 325 nm.[28] Spin-casting was used to coat each substrate with approximately 5 nm of CV to ensure it was within the evanescent field of the LSPR. Figure 1d compares the corresponding Raman Stokes spectra of CV from the three substrates after 180 s of signal averaging. Three well-known CV Raman features are clearly observed above a broad fluorescence band that increases with increasing wavelength. The peaks at 1172 cm^{-1}, 1383 cm^{-1}, and 1617 cm^{-1} are from C−H in-plane bending and two C−C stretching vibrational modes of the aromatic ring, respectively.[5,29,30] A comparison of the spectra taken from substrate regions without and with the Ga NPs graphically indicates that each substrate produces enhanced CV Raman signals and fluorescence for all three features (Figure 1d). Note that any resonant Raman enhancement affects both regions equally, and nonresonant Raman signals may exhibit an even stronger enhancement.[31] Because the reference and enhanced spectra are similar in form,[18] the enhancement observed is purely caused by the local plasmonic (and perhaps, though less likely, a charge transfer) effect.[32] After accounting for the fact that the Ga NP substrates have more surface area than bare sapphire,[33] a quantitative comparison of the strength of the Raman feature at 1617 cm^{-1} estimates the Raman enhancement factor η_R to be 5, 6, and 22 for the "blue", "resonant", and "red" substrates, respectively. The weak fluorescence between 329 and 355 nm (400−2600 cm^{-1} in Figure 1d) is similarly enhanced, with net fluorescence enhancement factors η_F of 2, 3, and 9, respectively.

Note that the enhancements are not strongest when the aggregate LSPR frequency coincides with the laser, suggesting a more complex process must be responsible for the enhancements observed. The fluorescence is enhanced by the increased absorption of the pump field near the NPs but is strongly suppressed at wavelengths where the fluorescence overlaps the LSPR.[34−37] This explains why the largest η_F occurs for the substrate with the largest NPs whose LSPR is not resonant with the fluorescence near 325 nm. It is interesting that this "red" substrate, with its bimodal size distribution, also produced the largest η_R. Similar visible wavelength SERS measurements of the analyte cresyl fast violet deposited on similar Ga NP substrates revealed that the "blue" substrate with the smallest, most tightly packed NPs (45 nm mean radius, 16 nm mean spacing) produced the largest η_R, followed by the "red" substrate with a bimodal size distribution.[38] Together, these observations suggest that enhancement occurs between NPs that are in close proximity in a manner that depends on excitation wavelength.

It has long been recognized that strong SERS and SEF signals may be measured from analyte in the small gap "hot spot" between two NPs whose coupling depends exponentially on their spatial separation.[39−41] This effect is responsible for the behavior seen in previous visible wavelength SERS measurements in which the coupled Ga NPs are of roughly equal size.[38] However, it was recently argued that a tightly coupled large and small metallic NP dimer constitutes a superior combination for enhanced optical scattering.[1,42] In this configuration, the larger NP acts as an enhanced absorbing

dx.doi.org/10.1021/nl401145j | Nano Lett. 2013, 13, 2837−2841

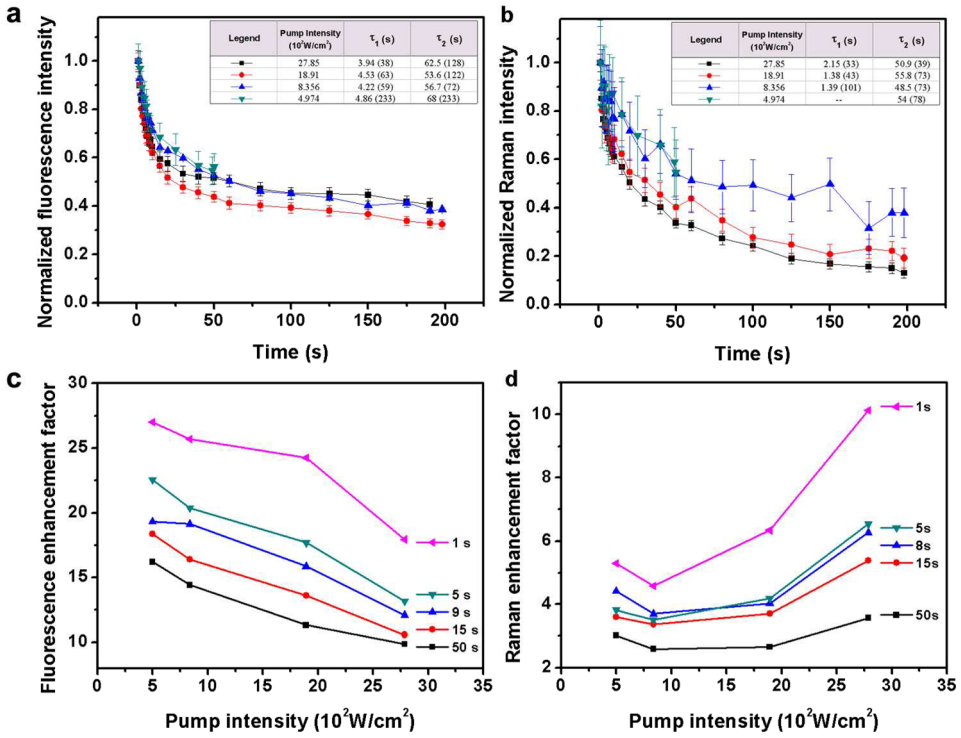

Figure 2. Temporal evolution of the fluorescence (a) and Raman (b) spectra for one-second exposures for four different pump intensities on the "red" substrate. Dependence of fluorescence (c) and Raman (d) enhancement factors on pump intensity for various exposure times, with uncertainties in η_F and η_R of 5% and 10%, respectively.

"antenna", while the smaller NP acts as a "resonator" enhancing the field strength, thereby providing a larger Raman enhancement than either NP can alone. This occurs most effectively in the "red" substrate, because of the bimodal distribution of small halo NPs surrounding and coupled to large NPs, and it is that substrate which exhibits the greatest η_F and η_R for UV SEF and SERS, respectively. Together, these observations suggest that under long wavelength (i.e., visible) illumination the small NPs with a unimodal size distribution are simultaneously large enough to be good absorbers but small enough to produce strong enhancements; however, as the illumination wavelength approaches the size of the NPs (i.e., UV), the asymmetric NP dimers accomplish both absorption and enhancement more effectively.

The observed enhancements appear modest because the reported values represent an aggregate enhancement over the entire distribution of CV-coated Ga NPs. By analyzing the spectra temporally and spatially, the distributions and contributions of the varied local enhancement factors may be ascertained. Spectra were retaken for 500 one-second exposures of the "red" substrate, and the temporal evolution of the fluorescence and Raman signals were plotted for four pump intensities in Figure 2a and b, respectively. Note that both signals rapidly decay, and a biexponential fit of the fluorescence and Raman decays reveals weakly pump intensity-dependent characteristic time scales on the order of τ_{fast} = 4, 2 and τ_{slow} = 60 and 50 s, respectively. (The actual values and uncertainties are given in the figures.) Clearly the UV laser is damaging the CV, particularly in the regions where the field concentration is highest, and the majority of the enhancement and damage occurs in the first few seconds.[43]

Because of the statistical distribution of particle sizes and spacings, the varied contributions of localized enhancement factors responsible for both strengthening the spectra and damaging the CV cannot be estimated ab initio. However, it may be estimated experimentally following the work of Fang et al. in which the intensity of the spectra are monitored as a function of pump intensity.[44,45] For a very weak excitation, well below the damage threshold of the CV, the spectra should not deteriorate with a 500 s exposure. As the pump intensity is increased, the field in hotspots with the largest enhancement factors will rise above the damage threshold, decreasing the Raman signal in proportion to the hotspot's contribution. Further increases in laser intensity will allow hotpots with weaker enhancement factors to reach the damage threshold, so a histogram of hotspot areal coverage and enhancement factor contribution may be ascertained through this method. Figure 3a plots the strength of the Raman signal for the "red" substrate as a function of $g = E_{th}/E$ after 500 one-second exposures, where E is the electric field strength from the laser intensity and E_{th} = 1.5 ± 0.3 MV/m is the measured photochemical damage threshold for CV. The latter was measured as the incident field strength at which the intensity of the Raman signal stopped varying linearly with pump intensity and is consistent with the 1.5 MV/m damage threshold of acrylic polymers measured using nanosecond pulsewidth UV laser pulses at 355 nm.[30,46] For the experiments performed, $g \gg 1$, reflecting a regime in which the laser intensity is well below the damage threshold so damage may only occur locally at hotspots. Based on the assumption that the local enhancement factor for Raman scattering goes as $\eta_R = g^4$,[4,44,47−49] the hotspot spatial distribution and corresponding Raman contribution may be obtained (Table 1). Note that 86% of the spectral strength comes from less than 3% of the surface area, and enhancement factors as large as 10^7 are observed in a few locations. Since we were not able to measure the weak Raman spectra for g > 50,

dx.doi.org/10.1021/nl401145j | Nano Lett. 2013, 13, 2837−2841

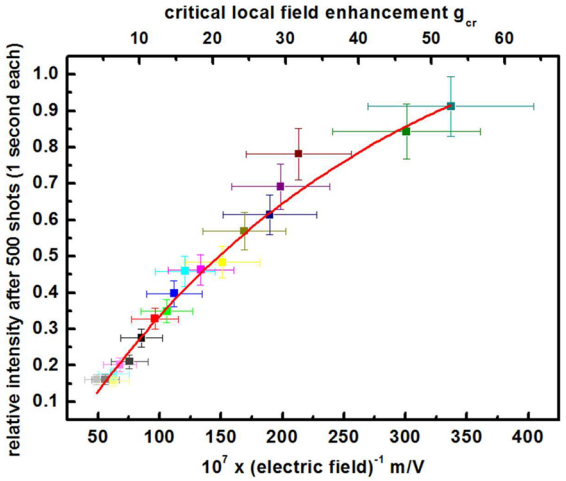

Figure 3. Raman intensity as a function of inverse pump field intensity normalized to the damage threshold of CV, measured to be 1.5 ± 0.3 MV/m. The characteristic inverse electric field strength for the fitted exponential is 200 ± 35 × 10^{-7} m/V.

Table 1. Contribution of the Various Site Enhancements at 325 nm to the Overall SERS Signal

Raman enhancement factor η_R	percentage of surface area	percentage contribution to SERS signal
$>10^7$	0.000088%	2.24%
10^6–10^7	0.0044%	24.2%
10^5–10^6	0.043%	25.3%
10^4–10^5	0.334%	20.3%
10^3–10^4	2.25%	14.0%
10^2–10^3	14.00%	8.78%
$<10^2$	83.37%	5.26%

the estimated enhancement factors are a lower bound, and there may be regions with even higher enhancement that were damaged even under our weakest illumination.

LSPR-enhanced SERS requires both the laser and Stokes Raman fields be enhanced simultaneously. UV Raman signals are closer in wavelength to the Rayleigh-scattered laser light than in the visible or near-IR, and the Ga NP LSPR is broader than the comparable LSPR from Ag or Au NPs. Consequently, the critical assumption upon which this analysis depends, namely $\eta_R = I_{SERS}/I_{in} \approx g^4$ (derived from $E_{abs} = gE_{in}$, $E_{SERS} \approx gE_{abs} = g^2E_{in}$, and $\eta_F = I_{abs}/I_{in} = g^2$ for incident, absorbed, and SERS-scattered fields E_i and intensities I_i, respectively) is more applicable in the UV than at lower energies.[8,50,51] Using the data from Figure 2a,b, the behavior of η_R and η_F may be plotted as a function of pump intensity at selected times (Figure 2c,d). Note that, for a given exposure time, η_F decreases with increasing time and with increasing power because of laser-induced damage at hotspots.[52] Given that, the increase in η_R with pump intensity confirms the significant contribution to the SERS signal from undamaged CV in the remaining hotspots below the laser damage threshold.

In conclusion, a UV plasmonic substrate of Ga NPs has been fabricated, and its utility for UV SERS, SEF, and SEPD has been demonstrated. Gallium NPs were deposited using MBE, and their collective LSPR was monitored in situ by SE so that deposition could be halted when the LSPR reached the desired frequency. Enhanced Raman and fluorescence spectra of CV deposited on these substrates were measured and quantitatively compared with the corresponding CV spectra on bare sapphire. The strongest enhancements were observed when the lower frequency LSPR mode was on the red side of the laser frequency. The modest fluorescence and Raman enhancements observed represent average values over the broad distribution of Ga NP sizes and separations. Actual local enhancements are much stronger, some in excess of 10^7, leading to a rapid temporal decay of the signals as analyte is damaged at these same hotspots. Techniques for fabricating ordered spatial arrays may allow Ga NPs to become the gold or silver standard for UV nanoplasmonic applications.

Methods. Ga NPs were deposited onto single-side polished sapphire substrates held at room temperature using a Veeco GEN II plasma-assisted molecular beam epitaxy system. Under ultrahigh vacuum conditions, the NPs were deposited at a constant Ga beam equivalent pressure of 2.0 × 10^{-7} Torr, corresponding to 19 nm/min of Ga in the thin-film approximation. Because of the low melting point ($T_m \sim 30$ °C) and the well-known undercooling of Ga NPs, liquid Ga NPs are formed by a self-organization process and solidify at room temperature, thereby avoiding any reaction with the substrate.[53] The bulk plasmon resonance of Ga is 14 eV, and the damping constant is 1.54 eV.[19] The imaginary part of its dielectric function spans ε_i = 5–12 over the 300–400 nm wavelength range of interest. During deposition, in situ grazing incidence spectroscopic ellipsometry (a UVISEL Jobin-Yvon spectrometer, 70° from normal, spanning the 1.5–6.0 eV region) was used to measure the pseudodielectric function of the collective surface effective medium composed of the metal NPs and the sapphire substrate.[20,25] The LSPR of the collective Ga NP ensemble monitored during deposition is revealed by modeling the response as a Lorentizan oscillator after subtracting the measured dielectric function of the bare sapphire substrate measured before deposition.[54,55]

To ensure uniformly thin coverage of the substrate NPs, CV from Sigma-Aldrich in 0.2 × 10^{-4} M ethanol solution was spin-cast onto a substrate at 1500 rpm at room temperature for 3 min to produce a 5 nm thick uniform coating. The substrates were dried for 15 min to ensure ethanol evaporation and minimize the distance between CV molecules and substrate surface. Atomic force microscopy (AFM) confirmed the uniformity of the conformal molecular layer that thinly coats the surface of the NPs. The laser beam was focused to a spot 8 μm in diameter. The spectra were collected by a confocal microscope with a 0.45 numerical aperture, diffracted using a 30 cm spectrometer with a 1200 groove/mm holographic grating blazed at 300 nm, and detected by a liquid nitrogen cooled Princeton Instruments, UV-coated CCD. Detector dark counts and cosmic ray spikes were subtracted for all spectra presented. The electric field strength (V/m) is calculated from the laser intensity I (W/m^2) using $E = (377\ I/2)^{1/2}$.[56]

AUTHOR INFORMATION

Notes

The authors declare no competing financial interest.

ACKNOWLEDGMENTS

This work was supported by the Army Aviation & Missile Research, Development, and Engineering Center and the Office of Naval Research. The authors thank the early contributions of Ga NP SERS, spin-casting of CV, and building the spectrometer by P. C. Wu, K. R. Lantz, and J. V. Foreman, respectively. The authors would like to thank Greg Sun, Dana

Dlott, Maria Losurdo, George Schatz, Fernando Moreno, Francisco Gonzalez, Pablo Albella, and Juan Marcos Sanz Casado for their insightful comments.

REFERENCES

(1) Sun, G.; Khurgin, J. B. *Appl. Phys. Lett.* **2011**, *98*, 3116.
(2) Fort, E.; Grésillon, S. *J. Phys. D: Appl. Phys.* **2007**, *41*, 013001.
(3) Anker, J. N.; Hall, W. P.; Lyandres, O.; Shah, N. C.; Zhao, J.; van Duyne, R. P. *Nat. Mater.* **2008**, *7*, 442−453.
(4) West, P. R.; Ishii, S.; Naik, G. V.; Emani, N. K.; Shalaev, V. M.; Boltasseva, A. *Laser Photon. Rev.* **2010**, *4*, 795−808.
(5) Kneipp, K.; Wang, Y.; Kneipp, H.; Perelman, L.; Itzkan, I.; Dasari, R.; Feld, M. *Phys. Rev. Lett.* **1997**, *78*, 1667−1670.
(6) Nie, S.; Emory, S. *Science* **1997**, *275*, 1102−1106.
(7) Jackson, J. B.; Halas, N. J. *Proc. Natl. Acad. Sci. U.S.A.* **2004**, *101*, 17930−17935.
(8) LeRu, E. C.; Blackie, E.; Meyer, M.; Etchegoin, P. G. *J. Phys. Chem. C* **2007**, *111*, 13794−13803.
(9) Khurgin, J. B.; Sun, G. *J. Opt. Soc. Am. B* **2009**, *26*, B83−B95.
(10) Ren, B.; Lin, X.; Yang, Z.; Liu, G.; Aroca, R.; Mao, B.; Tian, Z. *J. Am. Chem. Soc.* **2003**, *125*, 9598−9599.
(11) Chan, G. H.; Zhao, J.; Schatz, G. C.; van Duyne, R. P. *J. Phys. Chem. C* **2008**, *112*, 13958−13963.
(12) Chowdhury, M. H.; Ray, K.; Gray, S. K.; Pond, J.; Lakowicz, J. R. *Anal. Chem.* **2009**, *81*, 1397−1403.
(13) Watanabe, Y.; Inami, W.; Kawata, Y. *J. Appl. Phys.* **2011**, *109*, 023112.
(14) Mattiucci, N.; D'Aguanno, G.; Everitt, H. O.; Foreman, J. V.; Callahan, J. M.; Buncick, M. C.; Bloemer, M. J. *Opt. Express* **2012**, *20*, 1868−1877.
(15) Knight, M. W.; Liu, L.; Wang, Y.; Brown, L.; Mukherjee, S.; King, N. S.; Everitt, H. O.; Nordlander, P.; Halas, N. J. *Nano Lett.* **2012**, *12*, 6000−6004.
(16) Asher, S. A. *Annu. Rev. Phys. Chem.* **1988**, *39*, 537−588.
(17) Asher, S. A.; Ludwig, M.; Johnson, C. R. *J. Am. Chem. Soc.* **1986**, *108*, 3186−3197.
(18) Dörfer, T.; Schmitt, M.; Popp, J. *J. Raman Spectrosc.* **2007**, *38*, 1379−1382.
(19) Zeman, E. J.; Schatz, G. C. *J. Phys. Chem.* **1987**, *91*, 634−643.
(20) Wu, P. C.; Kim, T.-H.; Brown, A. S.; Losurdo, M.; Bruno, G.; Everitt, H. O. *Appl. Phys. Lett.* **2007**, *90*, 103119.
(21) Wu, P. C.; Losurdo, M.; Kim, T.-H.; Giangregorio, M.; Bruno, G.; Everitt, H. O.; Brown, A. S. *Langmuir* **2009**, *25*, 924−930.
(22) Vivekchand, S. R. C.; Engel, C. J.; Lubin, S. M.; Blaber, M. G.; Zhou, W.; Suh, J. Y.; Schatz, G. C.; Odom, T. W. *Nano Lett.* **2012**, *12*, 4324−4328.
(23) Taguchi, A.; Hayazawa, N.; Furusawa, K.; Ishitobi, H.; Kawata, S. *J. Raman Spectrosc.* **2009**, *40*, 1324−1330.
(24) Jha, S. K.; Ahmed, Z.; Agio, M.; Ekinci, Y.; Löffler, J. F. *J. Am. Chem. Soc.* **2012**, *134*, 1966−1969.
(25) Wu, P. C.; Losurdo, M.; Kim, T.-H.; Choi, O.; Bruno, G.; Brown, A. S. *J. Vac. Sci. Technol., B* **2007**, *25*, 1019−1023.
(26) Schatz, G. C.; Young, M. A.; van Duyne, R. P. *Top. Appl. Phys.* **2006**, *103*, 19−45.
(27) Albella, P.; Garcia-Cueto, B.; González, F.; Moreno, F.; Wu, P. C.; Kim, T.-H.; Brown, A.; Yang, Y.; Everitt, H. O.; Videen, G. *Nano Lett.* **2011**, *11*, 3531−3537.
(28) Galloway, C.; Etchegoin, P.; Le Ru, E. *Phys. Rev. Lett.* **2009**, *103*, 063003.
(29) Liang, E. J.; Ye, X. L.; Kiefer, W. *J. Phys. Chem. A* **1997**, *101*, 7330−7335.
(30) Canamares, M. V.; Chenal, C.; Birke, R. L.; Lombardi, J. R. *J. Phys. Chem. C* **2008**, *112*, 20295−20300.
(31) Sun, G.; Khurgin, J. *Phys. Rev. A* **2012**, *85*, 063410.
(32) Jiang, J.; Burstein, E.; Kobayashi, H. *Phys. Rev. Lett.* **1986**, *57*, 1793−1796.
(33) McFarland, A. D.; Young, M. A.; Dieringer, J. A.; van Duyne, R. P. *J. Phys. Chem. B* **2005**, *109*, 11279−11285.
(34) Gontijo, I.; Boroditsky, M.; Yablonovitch, E.; Keller, S.; Mishra, U.; DenBaars, S. *Phys. Rev. B* **1999**, *60*, 11564−11567.
(35) Neogi, A.; Lee, C.; Everitt, H.; Kuroda, T.; Tackeuchi, A.; Yablonovitch, E. *Phys. Rev. B* **2002**, *66*, 153305-1−4.
(36) Kühn, S.; Håkanson, U.; Rogobete, L.; Sandoghdar, V. *Phys. Rev. Lett.* **2006**, *97*, 153605.
(37) Sun, G.; Khurgin, J. B.; Tsai, D. P. *Opt. Lett.* **2012**, *37*, 1583−1585.
(38) Wu, P. C.; Khoury, C. G.; Kim, T.-H.; Yang, Y.; Losurdo, M.; Bianco, G. V.; Vo-Dinh, T.; Brown, A. S.; Everitt, H. O. *J. Am. Chem. Soc.* **2009**, *131*, 12032.
(39) Moskovits, M. *Rev. Mod. Phys.* **1985**, *57*, 783−826.
(40) García-Vidal, F. J.; Pendry, J. B. *Phys. Rev. Lett.* **1996**, *77*, 1163−1166.
(41) Le Ru, E. C.; Etchegoin, P. G.; Meyer, M. *J. Chem. Phys.* **2006**, *125*, 4701.
(42) Sun, G.; Khurgin, J. B. *Appl. Phys. Lett.* **2010**, *97*, 3110.
(43) Bjerneld, E. J.; Svedberg, F.; Johansson, P.; Käll, M. *J. Phys. Chem. A* **2004**, *108*, 4187−4193.
(44) Fang, Y.; Seong, N.-H.; Dlott, D. D. *Science* **2008**, *321*, 388−392.
(45) Fang, Y.; Yang, H.; Jiang, P.; Dlott, D. *J. Raman Spectrosc.* **2011**, *43*, 389−395.
(46) Maezono, Y.; Yousuke, I.; Kurosawa, K.; Katto, M.; Yokotani, A. *SPIE* **2006**, *6346*, 63462O−5.
(47) Kerker, M.; Wang, D. S.; Chew, H. *Appl. Opt.* **1980**, *19*, 3373−3388.
(48) Wang, D.; Kerker, M. *Phys. Rev. B* **1981**, *24*, 1777−1790.
(49) Stiles, P. L.; Dieringer, J. A.; Shah, N. C.; van Duyne, R. P. *Annu. Rev. Anal. Chem.* **2008**, *1*, 601−626.
(50) Xu, H.; Wang, X.-H.; Persson, M.; Xu, H.; Käll, M.; Johansson, P. *Phys. Rev. Lett.* **2004**, *93*, 243002.
(51) Franzen, S. *J. Phys. Chem. C* **2009**, *113*, 5912−5919.
(52) Etchegoin, P. G.; Lacharmoise, P. D.; Le Ru, E. C. *Anal. Chem.* **2009**, *81*, 682−688.
(53) Parravicini, G. B.; Stella, A.; Ghigna, P.; Spinolo, G.; Migliori, A.; D'Acapito, F.; Kofman, R. *Appl. Phys. Lett.* **2006**, *89*, 033123.
(54) Oates, T. W. H.; Sugirne, H.; Noda, S. *J. Phys. Chem. C* **2009**, *113*, 4820−4828.
(55) Oates, T. W. H.; Wormeester, H.; Arwin, H. *Prog. Surf. Sci.* **2011**, 1−49.
(56) Boyd, R. W. *Nonlinear optics*, 3rd ed.; Elsevier/Academic Press: Amsterdam, 2008; pp xx−613.